Displacive phase transitions in infinite-layer nickelates from first- and second-principles calculations

Yajun Zhang [1,2,*] Jingtong Zhang [3,4] Jiahang Li[1,2] M. P. K. Sahoo,[5] Xu He [6] Jie Wang [3,4] and Philippe Ghosez [6]

[1]*Key Laboratory of Mechanics on Disaster and Environment in Western China Attached to The Ministry of Education of China, Lanzhou University, Lanzhou 730000 Gansu, China*

[2]*Department of Mechanics and Engineering Science, College of Civil Engineering and Mechanics, Lanzhou University, Lanzhou 730000 Gansu, China*

[3]*Department of Engineering Mechanics and Key Laboratory of Soft Machines and Smart Devices of Zhejiang Province, Zhejiang University, 38 Zheda Road, Hangzhou 310027, China*

[4]*Zhejiang Laboratory, Hangzhou 311100, Zhejiang, China*

[5]*Department of Physics, Veer Surendra Sai University of Technology, Burla, Odisha, 768017, India*

[6]*Theoretical Materials Physics, Q-MAT, CESAM, Université de Liège, B-4000 Liège, Belgium*

Antiferrodistortive (AFD) motions in ABX_3 perovskites play an important role in determining, tuning, and creating functionalities. Here, through first-principles calculations, we predict that the AFD motions in RNiO$_2$ (where R denotes rare-earth ion), which recently gained significant interest as superconductor systems, show very similar behaviors with perovskites in various aspects, indicating an intrinsic property. The origin of AFD motions is rationalized by chemical bond valence theory, and we reveal that the undercoordination of the R cation is the driving force for the appearance of rotation, analogous to perovskites. Going further, the temperature dependence of local deformations is addressed by developing a second-principles model, and we suggest that the structural phase transitions should be classified as displacive. Eventually, a direct rotation-electron-spin connection is established, which opens a pathway to purposefully tune the Fermi surface, magnetic coupling strength, and magnetic dimensionality. Given that superconducting properties are associated with electronic and magnetic properties, our results provide the possibility and feasibility of the practical control of behaviors in nickelate superconductors through rotation engineering.

I. INTRODUCTION

Antiferrodistortive (AFD) motions, which normally include rotations and tilts, exist broadly in ABX_3 perovskites, and they have been identified as a powerful approach to control functional properties through the strong interplay with lattice, electron, and spin degrees of freedom [1–48]. From a structural point of view, AFD motions are the primary order parameter to induce ferroelectricity through a hybrid improper mechanism [1–10]. In addition, AFD motions can facilitate the design of polar metal [11–13] and magnetically induced multiferroics [14–20]. From an electronic point of view, AFD motions have been widely exploited as practical strategies to optimize properties such as band gap [21–25], metal-insulator transition of RNiO$_3$ (where R denotes rare-earth) and RMnO$_3$ [26–32], and even the superconductivity of cuprates [33–36]. From the viewpoint of magnetic properties, AFD motions have been revealed to be of direct relevance to magnetic interactions [37–39], Néel/Curie temperature [40–44], and magnetic order [45–48].

Infinite-layer nickelates RNiO$_2$, which are derived from the RNiO$_3$ perovskites by removing apical oxygen, have recently gained growing interest inspired by the discovery of superconductivity [49–78]. AFD rotations are important characteristics of RNiO$_3$ perovskite, which are not only critical for the appearance of a metal-insulator transition [26], but also are useful for a continuous fine-tuning of the transition temperature [27]. As infinite-layer RNiO$_2$ and RNiO$_3$ perovskites have the same atomic structure at the square plane, and rotation around the c axis only involves displacements of oxygen at the square plane, it is reasonable to expect that RNiO$_2$ may also have similar in-plane rotation.

In experiments, it is suggested that LaNiO$_2$ and NdNiO$_2$ are crystallized in the $P4/mmm$ phase without AFD motions [75,79]. Recently, several theoretical works have reported the appearance of in-plane rotation in RNiO$_2$ with small R-site cations [69–73]. Despite the progress on the structural properties, there is no clear explanation for the driving mechanisms of the structural transitions. Moreover, being able to determine whether dynamically stabilized phases are of an order-disorder or displacive nature is important for understanding material properties that depend on local structure [80–86]. Therefore, the understanding of the displacive or order-disorder transition is one of the central issues of condensed-matter physics. To our knowledge, the details of the characteristics of the local structure in RNiO$_2$ at different temperature have not been reported yet. More importantly, a robust understanding of the similarity and difference of rotation effects in infinite-layer RNiO$_2$ and RNiO$_3$ perovskites

*zhangyajun@lzu.edu.cn

has still not been achieved, which may impede the full exploitation of rotation engineering. It is well known that the electronic and magnetic properties have strong and direct connections with superconductivity [87–89]. Uncovering the origin and nature of rotation and disentangling the effects on the electronic and magnetic properties are fundamental to the rational optimization of superconducting critical temperatures.

In this work, the driving force for the oxygen rotation, its order-disorder or displacive nature, and the effects on the electronic and magnetic properties in infinite-layer nickelates are investigated by a combination of first- and finite-temperature second-principles calculations. The results unveil that the oxygen rotation of infinite-layer nickelates is strikingly similar to that witnessed in perovskites. We further reveal that oxygen rotation motion originates from the enhancement of R-O covalency due to the undercoordination of a smaller R-cation (R = Nd-Lu), which is also in line with perovskites. A finite-temperature second-principles model is constructed to describe temperature-dependent structural transformations. Our results provide evidence that rotation motion exhibits displacive characteristics. By investigating the change of electronic and magnetic properties induced by rotation motion, we establish a direct rotation-electron-spin link. The strong sensitivity of the Fermi surface, magnetic coupling strength, and magnetic dimensionality to rotation provides the potential to optimize superconducting properties by rotation engineering.

II. METHODS

A. First-principles calculations

First-principles density functional theory (DFT) calculations as implemented in the Vienna Ab initio Simulation Package (VASP) [90,91] were carried out to explore the ground-state properties. The Perdew-Burke-Ernzerhof functional revised for solid (PBEsol) [92] and Hubbard U [93] of 2.7 eV for the Ni $3d$ orbital were employed according to our previous work [73]. The plane-wave energy cutoff was set to be 700 eV. Brillouin zone integrations were performed using an $8 \times 8 \times 6$ Monkhorst-Pack k-point mesh [94] for a $\sqrt{2} \times \sqrt{2} \times 2$ supercell. Here, the energy of A-type antiferromagnetic (AFM), C-AFM, G-AFM, and ferromagnetic (FM) states was compared in the calculations to find the magnetic ground state. During the structural optimizations, the lattice constants and all internal atomic positions were fully relaxed until the Hellmann-Feynman force acting on each atom is less than 10^{-3} eV/Å. The exchange constants are calculated by using the TB2J code [95] based on the maximally localized Wannier functions [96,97]. The distortion amplitude is identified by the ISODISTORT software [98,99] relative to the distortion-free $P4/mmm$ phase.

B. Cristallochemical calculations of bond valence

To investigate the origin of rotations from a cristallochemical viewpoint, we considered a simple crystal chemical model based on the works of Brown [100,101] to calculate the R ion coordination in RNiO$_2$ and also RNiO$_3$ for comparison.
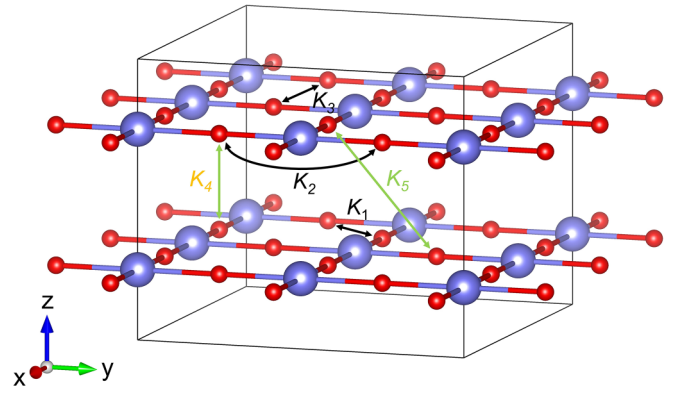

FIG. 1. Atomic structure of $P4/mmm$ HoNiO$_2$ and the schematic representation of five short-range interactions included in the energy term of the second-principles model.

According to their works, the bond valence sum V_R of cation R can be defined as

$$V_R = \sum_n s_{R\text{-}O_n} = \sum_n \exp\left(\frac{r_0' - r_{R\text{-}O_n}}{B}\right). \quad (1)$$

Here, $s_{R\text{-}O_n}$ denotes the valence of the bond between the cation R and the oxygen atom n, and r_0' is the bond valence parameter or nominal R-O bond length [102]. $r_{R\text{-}O_n}$ represents the actual bond length between the cation R and the oxygen atom n. For the empirical parameter B, the suggested value of 0.37 is used.

C. Finite-temperature second-principles calculations

A second-principles model for HoNiO$_2$ is built to study the behavior of structural distortions under different temperature. Since the rotation motion is only related to the change in the position of the oxygen atoms, we ignore the displacements of other atoms. Furthermore, we fixed the direction of movement of the oxygen atoms, since the degrees of freedom on two other directions do not participate in the A_4^- rotation mode. The high-symmetry phase $P4/mmm$ is selected as the reference structure, and total energy can be described by a Taylor expansion around the reference structure in the following way:

$$E_{\text{total}} = E_0 + \sum_i s_2 \mu_i^2 + \sum_i s_4 \mu_i^4 + \sum_{i \neq j} K_{ij} \mu_i \mu_j, \quad (2)$$

where μ_i is the displacement of the ith atom. For symmetry considerations, only even-order terms are kept. The $E_{\text{self}} = \sum_i s_2 \mu_i^2 + \sum_i s_4 \mu_i^4$ represents the energy of an isolated oxygen atom at the ith location. $E_{\text{short}} = \sum_{i \neq j} K_{ij} \mu_i \mu_j$ is the energy contribution from the short-range interactions between neighboring oxygen atoms. Here, five different short-range interactions and five K_{ij} (K_1, K_2, K_3, K_4, and K_5) are considered as sketched in Fig. 1.

To determine the parameters from first-principles calculations, we select 128 structures as the training set. The structures in the training set are $2 \times 2 \times 2$ supercell as shown in Fig. 1, and there are 16 oxygen atoms in one supercell. Since the direction of displacement is fixed, there are theoretically 2^{16} types of initial structures that need to be considered.

TABLE I. The parameters in Eq. (2) fitted from first-principles calculations. Here, the units of s_2, K_1, K_2, K_3, K_4, and K_5 are eV/Å^2 and the unit of s_4 is eV/Å^4.

s_2	s_4	K_1	K_2	K_3	K_4	K_5
0.3246	0.9657	0.0753	−0.0534	0.1013	0.0743	−0.0035

For the sake of simplicity, we force the oxygen atoms on the top layer to always move to the same or opposite direction to the oxygen atoms below it. Next, we only considered the structure to be symmetric about the x-axis. And finally, we reduce the number of initial structures with periodic boundary conditions. The number of initial structures is reduced from 2^{16} to 28. Among them, we choose eight structures that are closest to the rotation mode and linearly interpolate 16 structures between them and the $P4/mmm$ phase. The parameters are fitted with these 128 structures by minimizing the goal function:

$$G = \sum_{j=1}^{n} (E_{j,\text{model}} - E_{j,\text{DFT}})^2, \qquad (3)$$

where j runs from 1 to the number of structures in the training set, $E_{j,\text{model}}$ is the total energy obtained from the second-principles model for the jth structure, and $E_{j,\text{DFT}}$ is the energy from DFT calculations. All the parameters are listed in Table I. The total energy of the training set from our second-principles model is very close to that of DFT calculations (see Fig. S1 of the Supplemental Material [103]). Moreover, the curvatures of the potential energy surface (PES) of eight models from the two calculations agree well with each other, indicating that the second-principles model could also accurately describe the phonon frequency of each selected mode.

Based on the second-principles model, the Monte Carlo simulations are carried out on $16 \times 16 \times 16$ supercells to investigate the atomic movements at different temperatures. The simulations begin at 5 K, and they proceed in steps of 1 K increments until the temperature reaches 2100 K. For each temperature, 2×10^5 MC steps are used. During the simulations, the step sizes are adjusted to ensure an acceptance ratio of approximately 0.2. After we have obtained the equilibrium structure at different temperatures, 10^6 MC steps are performed to obtain the distribution of u_i.
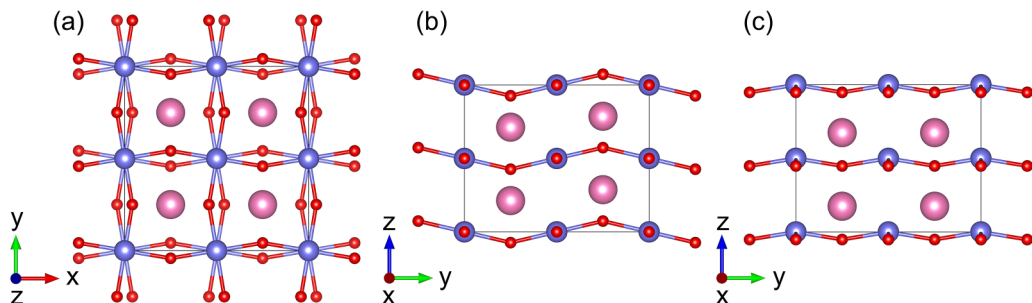

FIG. 3. PESs of out-of-phase rotation for RNiO$_2$ (R = La, Pr, Nd, Sm, Ho, and Lu).

III. RESULTS AND DISCUSSION

A. Intrinsic antiferrodistortive rotation

First, we concentrate on the AFD rotation instability in the high-symmetry $P4/mmm$ RNiO$_2$ by analyzing the PES of the rotation motion [see Fig. 2(a)]. The lattice constants of the $P4/mmm$ phase are fixed as the corresponding values in their bulk materials. The ground-state structure and magnetic order of the RNiO$_2$ series can be found in Ref. [73]. The calculations have been performed with the ground-state magnetic order, namely G-AFM for LaNiO$_2$ and PrNiO$_2$, and C-AFM for NdNiO$_2$, SmNiO$_2$, HoNiO$_2$, and LuNiO$_2$. Clearly, LaNiO$_2$ and PrNiO$_2$ are dynamically stable as shown in Fig. 3, while NdNiO$_2$, SmNiO$_2$, HoNiO$_2$ and LuNiO$_2$ exhibit the double-well PES, indicating the instability of rotation motion.

Although oxygen-square rotation in RNiO$_2$ has not been detected experimentally from neutron powder diffraction [79] and atomic-resolution high-angle annular dark-field (HAADF) STEM [75], these techniques are known to be less sensitive to light elements such as oxygen. The detection of oxygen-square rotation requires more relevant and efficient techniques such as atomic-resolution annular bright field (ABF) STEM [104] and integrated differential phase contrast

FIG. 2. Schematic representation of the (a) oxygen rotation motion (irreps A_4^-), tilt distortion (irreps X_2^-), and (c) polar distortion (irreps Γ_3^-).
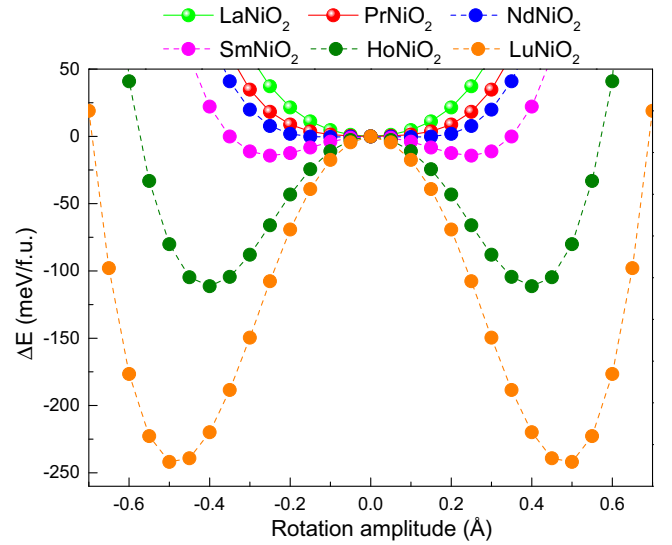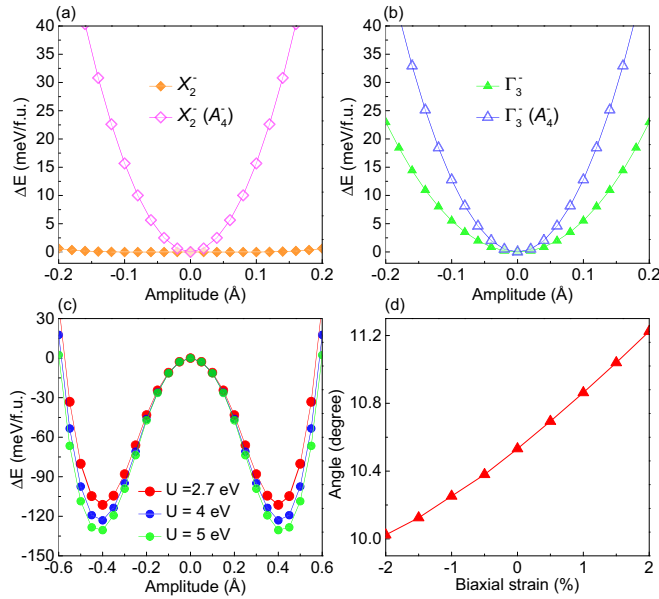
FIG. 4. Similarity between RNiO$_2$ and RNiO$_3$ from structural and chemical viewpoints. The PESs for the (a) X_2^- tilt distortion and (b) out-of-plane polarization Γ_3^- in HoNiO$_2$ with and without fixed rotation (A_4^-) of the ground-state value. (c) The PESs of out-of-phase rotation in HoNiO$_2$ as a function of Hubbard U. (d) The amplitude of rotation angle in HoNiO$_2$ as a function of epitaxial biaxial strain.

(iDPC) STEM [105]. We strongly suggest a thorough reexamination of lattice instability in the RNiO$_2$ system since we found that the intrinsic features of rotation motion in RNiO$_2$ infinite layer compounds are similar to the physics of related RNiO$_3$ compounds, and more generally of ABX_3 perovskites.

(i) *A-site ionic radius effect.* It is well known that rotation in ABX_3 perovskites is closely correlated to the *A*-site ionic radius. Typically, the amplitude of rotation monotonically increases with decreasing the ionic radius [26]. Comparing the curvature of PESs of RNiO$_2$ (R = Nd, Sm, Ho, and Lu) and their rotation amplitude with the lowest energy as shown in Fig. 3, it is obvious that rotation behaves in a strikingly similar fashion as in ABX_3 perovskite: decreasing ionic radius r_R simultaneously increases the instability and amplitude of rotation.

(ii) *Lattice competition between different rotation motions.* In many distorted ABX_3 perovskites, there are rotation motions along three directions with the $a^-a^-a^-$ or $a^-a^-c^+$ rotation pattern represented by Glazer notations [106]. Another feature of rotation motion is that rotation along a different direction tends to suppress each other [107]. From the PESs shown in Fig. 4(a), it is obvious that the out-of-phase A_4^- rotation enhances the stability of X_2^- tilt distortion [see Fig. 2(b)], indicating the strong competition between different rotation motions.

(iii) *Ferroelectricity-rotation lattice competition.* The competition between ferroelectric polarization and rotation is a rather generic behavior in ABX_3 perovskites and is responsible for the scarcity of ferroelectricity [108–110]. From the PESs of out-of-plane polar motion P_z [see Fig. 2(c)] of HoNiO$_2$ with and without rotation shown in Fig. 4(b), we confirm that polar motion becomes more stable and in-

creases the total energy due to the ferroelectricity-rotation competition.

(iv) *Covalency-dependent rotation.* In ABX_3 perovskites like CaFeO$_3$, Cammarata *et al.* point out that covalency of the metal-oxygen is strongly related to the rotation amplitude, and the more covalent the Fe-O bond is, the smaller is the rotation amplitude [111]. In addition, they found that Hubbard U can be considered as an indicator to track the evolution of covalency. Typically, the larger the U value, the weaker the covalency. To explore covalency-dependent rotation, we use a similar method and analyze the PESs of rotation in HoNiO$_2$ as a function of U. One can clearly see from Fig. 4(c) that increasing the U value continuously enhances the rotation instability, which is also in line with perovskites [111].

(v) *Strain-rotation coupling.* The fifth feature of rotation in ABX_3 perovskites is the strong coupling with epitaxial strain [112,113]. The amplitude of rotation is usually very sensitive to strain. We then examine the evolution of the rotation amplitude of HoNiO$_2$ with epitaxial strain ranging from -2% to 2%. A monotonic increase of rotation amplitude from compressive to tensile strain is clearly visible in Fig. 4(d). Obviously, such strong strain-rotation coupling is again similar with ABX_3 perovskites.

Although the Ni-O network is different in perovskite and the infinite layer, all these results confirm that RNiO$_2$ infinite layer compounds show a marked resemblance to that of ABX_3 perovskites from both structural and chemical viewpoints, providing further evidence that rotation instability should be an intrinsic feature of ABX_2 compounds. It is well known that there are plenty of approaches to tune the rotation of perovskites such as strain engineering, chemical doping, and interfacial coupling. The close parallelism between oxygen-square rotation in RNiO$_2$ compounds and oxygen octahedra rotation in RNiO$_3$ perovskites indicates that the strategies currently used in perovskites could be exploited in infinite layers to achieve the continuous control of rotation motion and related functional properties. In practice, relying then on chemical doping, we highlight in the following that the tuning of their ground-state properties and phase transitions could be realized.

B. Origin of AFD rotation from bond valence theory

We further disentangle the underlying physical origin of rotation motion from atomistic and crystal chemical viewpoints. The appearance of rotation motion in perovskites can be traced back to the seminal work of Pauling in 1929, in which it was proposed that the role of atomic motions was to optimize the coordination environment of anion about the *A*-site cation and find the minimum in the crystal energy [114]. Thus, the appearance and amplitude of rotation are determined by the best optimization of the coordination environment [106,115]. According to Brown [100,101], the bond valence sum V_R is a reliable fingerprint to describe the coordination environment.

In terms of RNiO$_2$, if the high-symmetry $P4/mmm$ phase is a metastable state, due to the undercoordination of the R cation, the oxygen atoms should move closer to the R cation to better coordinate the R-site cation and improve the R-O interactions. From this perspective, the difference of V_R between the high-symmetry and low-symmetry ground-state phases
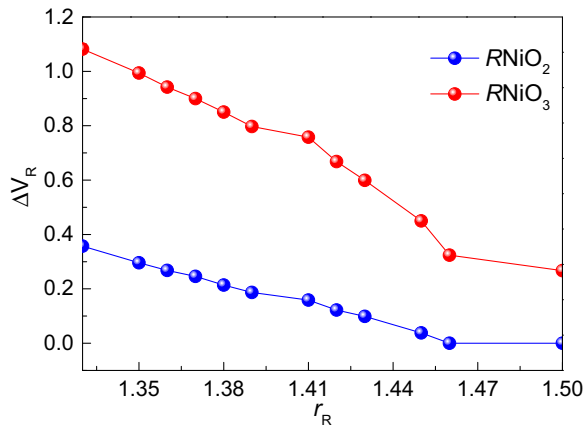
FIG. 5. The difference of bond valence sum V_R of cation R between the $P4/mmm$ and $I4/mcm$ phases (blue curve); the corresponding difference of V_R in RNiO$_3$ between cubic and $P2_1/c$ phases (red curve) are shown for comparison.

will be beneficial for the understanding of AFD rotation motion. The top view of RNiO$_2$ with rotation motion is displayed in Fig. 2(a). It is obvious that each cation R is surrounded by eight oxygen atoms. With the appearance of out-of-phase rotation motion, four oxygen atoms move closer to cation R in a same way as $a^0a^0c^-$ rotation in ABX_3 perovskites.

Figure 5 compares the difference of V_R in RNiO$_2$ between the $P4/mmm$ and $I4/mcm$ phases and RNiO$_3$ between the cubic and $P2_1/c$ phases in the FM order for simplicity. As the ground state of LaNiO$_2$ and PrNiO$_2$ is the high-symmetry $P4/mmm$ phase without rotation motion, the ΔV_R is zero for the two compounds. The results clearly reflect two similar features: (i) the V_R of high-symmetry phases in RNiO$_2$ (R = Nd-Lu) and RNiO$_3$ are smaller than the ground-state phases, and consequently AFD motions are favored to further enhance the covalency. The larger difference in RNiO$_3$ indicates strong AFD motions. This is consistent with the $a^-a^-a^-$ or $a^-a^-c^+$ AFD pattern with a much larger Ni-O-Ni bond angle along three directions, while RNiO$_2$ have a relatively smaller bond angle along two in-plane directions. (ii) The difference of V_R between the high-symmetry and low-symmetry phases increases continuously when the R cation radius decreases, suggesting much larger AFD motions are needed to optimize the coordination environment. This finding is also in line with the above discussion that RNiO$_2$ with a smaller R cation have stronger AFD instability and larger amplitudes of AFD motions, which is in accordance with ABX_3 perovskites.

In perovskites, it is known that lattice strain could also affect the instability of rotation through strain-rotation coupling. On decreasing the R cation radius, the lattice constants gradually decrease. To properly account for the lattice effects, we first analyze the variety of PES in which the rare-earth element La is kept the same and the lattice constants are changed to the values in a series of RNiO$_2$ compounds. It is clearly shown in Fig. 6(a) that the increase of compressive lattice strain dramatically increases the stability of rotation motion, which means that rotation is disfavored by the lattice strain induced by the reduction of the R cation radius. We then froze the lattice constants to that of LaNiO$_2$ and changed the
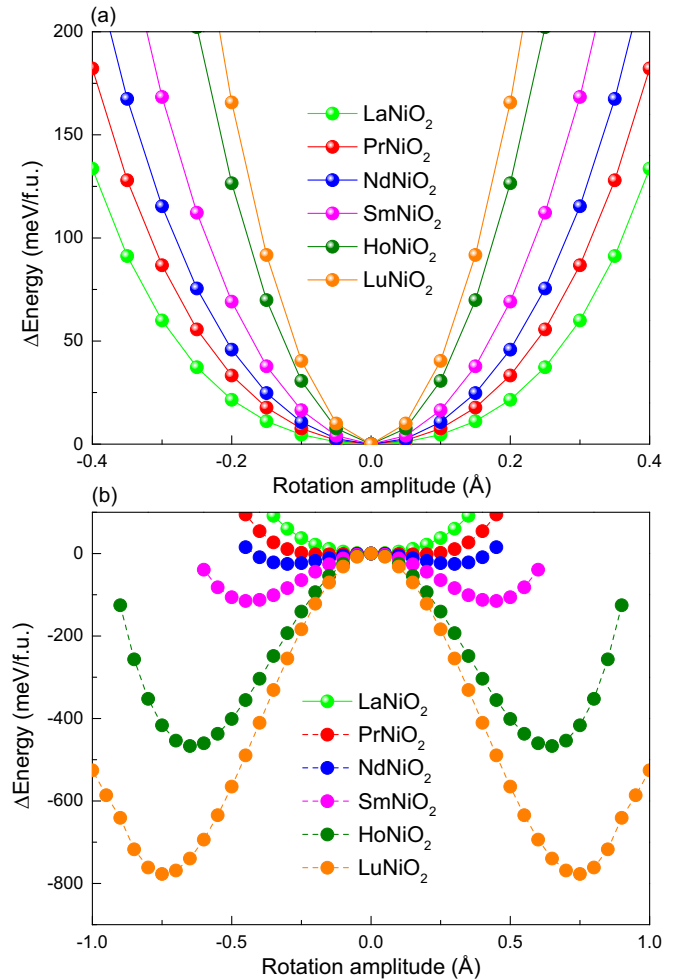

FIG. 6. (a) Comparison of the PESs of LaNiO$_2$ with the lattice constants of $P4/mmm$ LaNiO$_2$, PrNiO$_2$, NdNiO$_2$, SmNiO$_2$, HoNiO$_2$, and LuNiO$_2$. (b) Comparison of the PESs of RNiO$_2$ (R = La, Pr, Nd, Sm, Ho, and Lu) with the lattice constants of LaNiO$_2$.

R cation to a different element. Comparing with the results in Fig. 3, the curvatures of the PESs in Fig. 6(b) become more negative, and the rotation amplitude with the lowest energy notably increases for the same compounds, suggesting the enhancement of rotation instability by tensile lattice strain. Therefore, the bond valence effect outweighs the opposing effect of the decrease of lattice constants going through the RNiO$_2$ series, and provides a vivid crystal chemistry explanation for the origin of the AFD motion and the evolution trends. This finding suggests that AFD instability might be a general feature of all the ABX_2 compounds. It is worth noting that all previous experimental works report the high-symmetry $P4/mmm$ phase in RNiO$_2$ compounds [49,75,79], while several recent works have suggested the appearance of rotation motion [69–73]. The clear crystal chemistry explanation for the driving mechanisms of the structural transitions as found in perovskites might help resolve this apparent disagreement between experiments and theoretical calculations. Therefore, our results would provide a strong motivation for experimentalists to reexamine the structural instability.
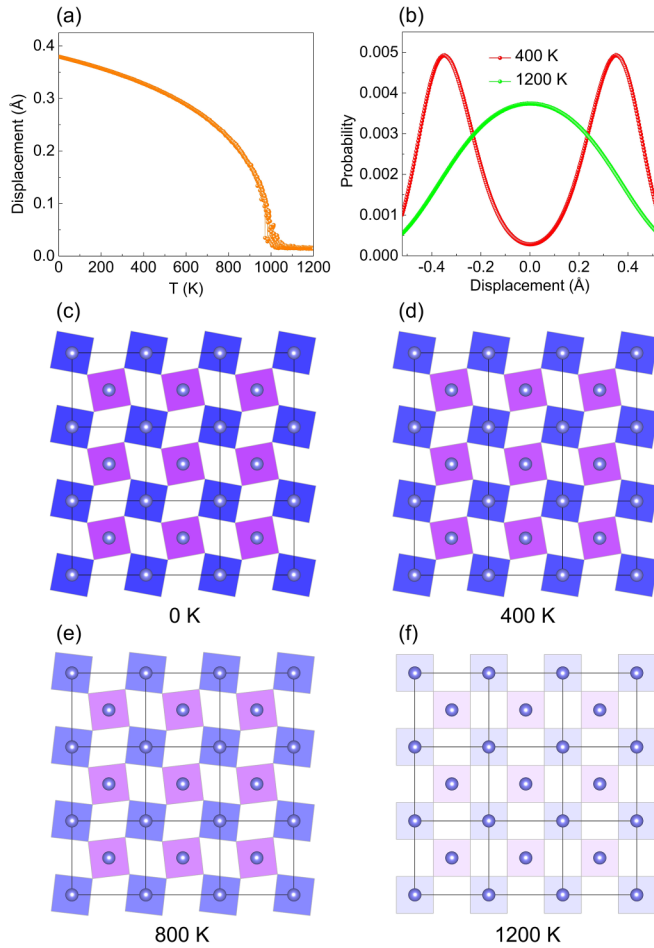
FIG. 7. Finite-temperature properties of HoNiO$_2$. (a) Temperature dependence of rotation motion related displacement of oxygen atoms relative to their high-symmetry positions. (b) The probability distribution of the real-space oxygen displacement in the high-symmetry $P4/mmm$ phase below (400 K) and above (1200 K) the transition temperature. The distribution of oxygen rotation motion at (c) 0 K, (d) 400 K, (e) 800 K, and (f) 1200 K. The shades of color represent the relative amplitude of rotation motion.

C. Displacive nature of structural phase transition

Having demonstrated the appearance and origin of rotation motion in RNiO$_2$ infinite layer compounds, it is natural to wonder about the displacive [85] or order-disorder [116] nature of rotation and behaviors at finite temperature. To answer these questions, we take HoNiO$_2$ as a model system and develop a second-principles model [117] by taking the displacements of oxygen atoms as the order parameter. The second-principles model is based on the fitted parameter from first-principles calculations, and it has recently been successfully used to capture the phase transitions in perovskites [118–120]. Moreover, a similar model is capable of disentangling the displacive or order-disorder characteristic of the phase transition [121,122].

Figure 7(a) shows the displacements of oxygen atoms relative to the high-symmetry position as a function of temperature. The $P4/mmm$-$I4/mcm$ transition occurs around 1000 K. To assess the mechanism of the phase transition, we

have explored the probability distribution of oxygen displacements in HoNiO$_2$ below and above the transition temperature. For a displacive transition, the distribution of distortion above the transition temperature is characterized by a unimodal with the maximum corresponding to the high-symmetry structure. In contrast, for compounds that undergo an order-disorder transition, the distribution of distortion is multimodal in the high-temperature phase with two symmetrically equivalent low-symmetry phases. The high-symmetry structure results from the dynamical average of the low-symmetry phases.

As displayed in Fig. 7(b), the distribution evolves from double peaks below T_R to a single peak centered at zero above T_R, which is indicative of a displacive characteristic. Figures 7(c)–7(f) display the distribution of oxygen rotation motion at different temperatures. Spatially homogeneous distributions are clearly visible, confirming that the phases are relatively ordered at each temperature. The amplitude of the distortion is progressively reduced as the temperature increases and disappears above T_R. Therefore, the rotation motion controlled structural transition in infinite-layer nickelates should be classified as a displacive transition, similar to the results of rotation in SrTiO$_3$ [85]. In an order-disorder transition, the temperature dependence of the order parameter is determined by the changes in the site occupations, not changes in the distortion amplitude. The demonstration of a displacive nature provides the theoretical basis for the continuous tuning of rotation motion and related advanced functions by external strategies. Additionally, the displacive nature of rotation motion combined with the temperature-dependent mode amplitude provides strong support to the phase transition triggered resistivity anomaly [49,73]. The order-disorder or displacive nature of the structural phase transition in perovskite has been extensively investigated; however, controversial conclusions can be obtained by different experimental measurements. Our demonstration of the displacive mechanism of the transition would provide important guidance for experimentalists to measure the rotation motion using appropriate equipment.

D. Tunable phase transitions by rotation engineering

The displacive nature of rotation distortion in RNiO$_2$ offers a unique opportunity to control desired properties by rotation engineering [27]. In the following, we highlight that the interesting electronic and magnetic transitions can be realized by continuously tuning the rotation amplitude. Taking widely investigated PrNiO$_2$ and NdNiO$_2$ nickelates as prototypical examples, we explain the concept of rotation engineering by establishing a direct rotation-electron-spin relationship.

Figure 8(a) presents the projected density of states (PDOS) of PrNiO$_2$ and NdNiO$_2$. The Fermi energy of PrNiO$_2$ is mainly occupied by the Ni $d_{x^2-y^2}$ bands, while the states of NdNiO$_2$ at the Fermi level mainly comprise Ni $d_{3z^2-r^2}$ bands. According to our previous work, the in-plane magnetic interactions are determined by the coupling between Ni $d_{x^2-y^2}$ bands, and the out-of-plane magnetic interactions are associated with the spin-polarized Ni $d_{3z^2-r^2}$ bands [73]. As a result, PrNiO$_2$ and NdNiO$_2$ exhibit quasi-2D and -3D magnetic dimensionality, respectively. As the relative energy level of Ni $d_{x^2-y^2}$ and $d_{3z^2-r^2}$ orbitals is the key for the
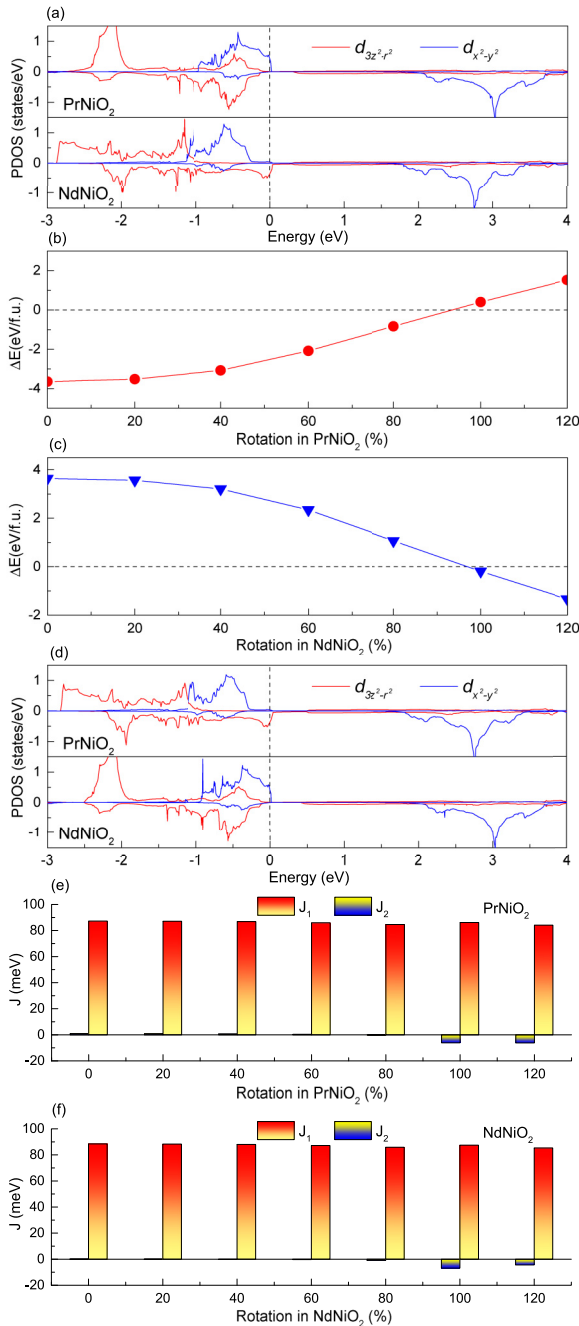
FIG. 8. Triggering electronic and magnetic transitions by rotation engineering. (a) The PDOS of Ni in $PrNiO_2$ and $NdNiO_2$. Rotation amplitude-dependent energy difference between the C-AFM and G-AFM reference phases in (b) $PrNiO_2$ and (c) $NdNiO_2$; here, 100% rotation corresponds to the rotation in the ground-state structure of $NdNiO_2$. (d) The PDOS of Ni for initially 2D-AFM $PrNiO_2$ with 120% of the rotation of $NdNiO_2$, and for initially 3D C-AFM $NdNiO_2$ with 60% of its rotation in the ground state. First-neighbor in-plane and out-of-plane exchange constants of (e) $PrNiO_2$ and (f) $NdNiO_2$ as a function of rotation motion.

magnetic dimensionality, it seems plausible that pushing down the band edge of the $d_{3z^2-r^2}$ orbital below the Fermi level would make 3D C-AFM $NdNiO_2$ more analogous to $CaCuO_2$, which has a 2D-AFM state. Under such a scenario, the $d_{3z^2-r^2}$

orbitals would be nearly fully occupied and the states around the Fermi level would be mainly dominated by the single Ni $d_{x^2-y^2}$ bands. On the contrary, for quasi-2D AFM $PrNiO_2$ with $d_{x^2-y^2}$ electrons at the Fermi level, pushing up the band edge of $d_{3z^2-r^2}$ orbital to cross the Fermi level is expected to trigger a transition from the quasi-2D AFM state to the 3D C-AFM state.

In perovskites, the increase (decrease) of in-plane rotation typically decreases (increases) the energy level of the in-plane $d_{x^2-y^2}$ orbital (out-of-plane $d_{3z^2-r^2}$ orbital) due to the weakening (enhancement) of the hybridization between Ni d orbitals and oxygen p orbitals. Here, we demonstrate that the mechanism still holds for infinite-layer compounds.

Figures 8(b) and 8(c) show the energy difference between 3D C-AFM and G-AFM states in $PrNiO_2$ and $NdNiO_2$ as a function of rotation. As can be found in Fig. 8(b), increasing the rotation amplitude in $PrNiO_2$ could trigger a magnetic transition from the G-AFM to the C-AFM state. On the contrary, the magnetic order of initial 3D C-AFM $NdNiO_2$ has changed to the G-AFM state with the decrease of rotation [see Fig. 8(c)].

To better understand the effect of rotation on the magnetic order, we compute the electronic structure of $PrNiO_2$ with 120% rotation of $NdNiO_2$ and $NdNiO_2$ with 60% rotation of its amplitude. The results, displayed in Figs. 8(a) and 8(d), indicate that increasing rotation has a strong effect on the band edge and Fermi surface; the dominated states at the Fermi level in $PrNiO_2$ have changed from $d_{x^2-y^2}$ bands to $d_{3z^2-r^2}$ bands. As expected, the change of the Fermi surface and spin polarization of the $d_{3z^2-r^2}$ bands gives rise to a pronounced jump of the first-neighbor out-of-plane exchange constant to sizable values [see Fig. 8(e)]. Despite the fact that J_1 is still small compared with J_2, it is able to induce notable dispersion along the out-of-plane wave-vector direction [123], which gives direct evidence for the 2D-3D magnetic transitions. In terms of $NdNiO_2$, the decrease in rotation increases the energy level of Ni $d_{x^2-y^2}$ orbitals to higher energy relative to the $d_{3z^2-r^2}$ orbitals. Consequently, the $d_{x^2-y^2}$ bands govern the Fermi level, and the spin polarization of $d_{3z^2-r^2}$ bands is suppressed [see Fig. 8(d)]. As the spin-polarized $d_{3z^2-r^2}$ bands are responsible for the out-of-plane magnetic couplings, the first-neighbor out-of-plane exchange constant becomes negligible for smaller rotation amplitude [see Fig. 8(f)], and eventually results in the 3D-2D magnetic transitions. The basic concept of the rotation-electron-spin relationship is illustrated in Fig. 9. The control of rotation amplitude strongly influences the competing on-site energy and band edge of the $d_{x^2-y^2}$ bands and $d_{3z^2-r^2}$ bands. By varying the rotation amplitude, one can delicately tune the electronic and magnetic transitions.

The rotation-controlled phase transitions can be naturally extended to practical systems. $Nd_{0.5}La_{0.5}NiO_2$ is chosen as model material to demonstrate the effectiveness of rotation engineering. $NdNiO_2$ is expected to undergo phase transitions to a 2D AFM state with $d_{x^2-y^2}$ bands at the Fermi level upon the half-doping of La due to the suppression of rotations. The energy of all possible structures with different arrangements of La and Nd is compared in Fig. S2 [103]. The comparison of electronic structures of $NdNiO_2$ in Fig. 7(a) and the lowest-energy structure of $Nd_{0.5}La_{0.5}NiO_2$ shown in Fig. S3 [103]
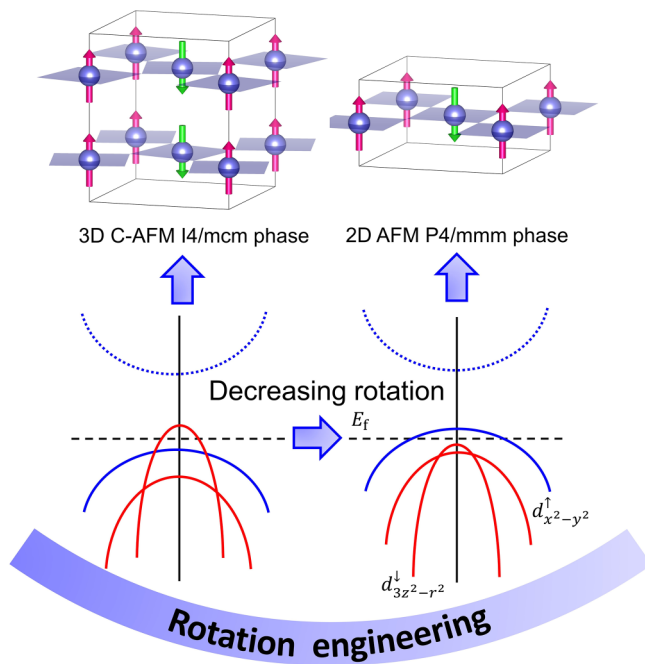
FIG. 9. Design concept for triggering electronic and magnetic transitions by rotation engineering.

IV. CONCLUSIONS

In conclusion, we have presented a systematic theoretical investigation of the rotation motion in infinite-layer nickelates using a combination of first- and second-principles calculations. We found intriguing similarities between the behaviors of rotation motion of infinite-layer nickelates and perovskites. We propose that the rotation motion is driven by the undercoordination of the R cation in the high-symmetry phase, and the difference in bond valence sum between the high-symmetry and the ground-state structure scales with the variance in the radii of the R cation, indicating stronger rotation in systems with a smaller rare-earth ion analogous to perovskites. The displacive nature of rotation is further explicitly confirmed by comparing the probability distribution of oxygen displacements below and above the transition temperature. Furthermore, we demonstrate that the Fermi surface and exchange interactions are highly sensitive to rotation motion. Rotation controlled electronic and magnetic transitions are rationalized by the establishment of a rotation-electron-spin relationship. We hope that our results could motivate further experiments to verify the existence and effect of AFD motions in $R\text{NiO}_2$ compounds and other ABX_2 system.

indicates that electronic transition occurs with half-doping of La and the Fermi surface is now dominated by the $d_{x^2-y^2}$ bands. The first-neighbor in-plane exchange constant is 18 times that of the out-of-plane exchange constant, confirming our expectation of the 3D-2D magnetic transition. The single $d_{x^2-y^2}$ band, strong orbital splitting between $d_{x^2-y^2}$ and $d_{3z^2-r^2}$ bands, and 2D magnetic interactions are commonly believed to be critical factors affecting the superconducting temperature T_c [87–89]. Establishing the connection between different factors and T_c is beyond the scope of the present work. Our results have provided intriguing insight into how to control the Fermi surface, orbital splitting, and magnetic interactions by rotation engineering. We hope that if further work could shed light on the exact connection, our work would be an important guide for the optimization of T_c through rotation engineering.

[1] N. A. Benedek and C. J. Fennie, Phys. Rev. Lett. **106**, 107204 (2011).

[2] N. A. Benedek and M. A. Hayward, Annu. Rev. Mater. Res. **52**, 331 (2022).

[3] A. Stroppa, P. Barone, P. Jain, J. M. Perez-Mato, and S. Picozzi, Adv. Mater. **25**, 2284 (2013).

[4] Y. S. Oh, X. Luo, F.-T. Huang, Y. Wang, and S.-W. Cheong, Nat. Mater. **14**, 407 (2015).

[5] H. J. Zhao, J. Iniguez, W. Ren, X. M. Chen, and L. Bellaiche, Phys. Rev. B **89**, 174101 (2014).

[6] E. Bousquet, M. Dawber, N. Stucki, C. Lichtensteiger, P. Hermet, S. Gariglio, J.-M. Triscone, and P. Ghosez, Nature (London) **452**, 732 (2008).

[7] Y. Zhang, M. P. K. Sahoo, T. Shimada, T. Kitamura, and J. Wang, Phys. Rev. B **96**, 144110 (2017).

[8] A. T. Mulder, N. A. Benedek, J. M. Rondinelli, and C. J. Fennie, Adv. Funct. Mater. **23**, 4810 (2013).

[9] Y. Zhang, J. Wang, and P. Ghosez, Phys. Rev. Lett. **125**, 157601 (2020).

[10] S. Dong, H. Xiang, and E. Dagotto, Natl. Sci. Rev. **6**, 629 (2019).

[11] T. Kim, D. Puggioni, Y. Yuan, L. Xie, H. Zhou, N. Campbell, P. Ryan, Y. Choi, J.-W. Kim, J. Patzner *et al.*, Nature (London) **533**, 68 (2016).

[12] S. Bhowal and N. A. Spaldin, Annu. Rev. Mater. Res. **53**, 53 (2023).

[13] S. Lei, M. Gu, D. Puggioni, G. Stone, J. Peng, J. Ge, Y. Wang, B. Wang, Y. Yuan, K. Wang *et al.*, Nano Lett. **18**, 3088 (2018).

[14] E. Bousquet and A. Cano, J. Phys.: Condens. Matter **28**, 123001 (2016).

[15] S. Picozzi, K. Yamauchi, I. A. Sergienko, C. Sen, B. Sanyal, and E. Dagotto, J. Phys.: Condens. Matter **20**, 434208 (2008).

[16] M. Mochizuki, N. Furukawa, and N. Nagaosa, Phys. Rev. Lett. **105**, 037205 (2010).

[17] Y. Tokura and S. Seki, Adv. Mater. **22**, 1554 (2010).

[18] E. Bousquet and A. Cano, Phys. Sci. Rev. **8**, 479 (2021).

[19] I. A. Sergienko, C. Şen, and E. Dagotto, Phys. Rev. Lett. **97**, 227204 (2006).

[20] Y. Tokura, S. Seki, and N. Nagaosa, Rep. Prog. Phys. **77**, 076501 (2014).

[21] W. Li, S. Niu, B. Zhao, R. Haiges, Z. Zhang, J. Ravichandran, and A. Janotti, Phys. Rev. Mater. **3**, 101601(R) (2019).

[22] M. R. Filip, G. E. Eperon, H. J. Snaith, and F. Giustino, Nat. Commun. **5**, 5757 (2014).

[23] Y. Zhang, M. Sahoo, Y. Liang, and G. Tang, J. Phys. Chem. Lett. **13**, 9632 (2022).

[24] A. Amat, E. Mosconi, E. Ronca, C. Quarti, P. Umari, M. K. Nazeeruddin, M. Gratzel, and F. De Angelis, Nano Lett. **14**, 3608 (2014).

[25] W. Zhang, G. Tang, M. P. K. Sahoo, Y. Liang, and Y. Zhang, Phys. Rev. B **105**, 075150 (2022).

[26] A. Mercy, J. Bieder, J. Íñiguez, and P. Ghosez, Nat. Commun. **8**, 1677 (2017).

[27] Z. Liao, N. Gauquelin, R. J. Green, K. Müller-Caspary, I. Lobato, L. Li, S. Van Aert, J. Verbeeck, M. Huijben, M. N. Grisolia *et al.*, Proc. Natl. Acad. Sci. (USA) **115**, 9515 (2018).

[28] Y. Zhang, M. M. Schmitt, A. Mercy, J. Wang, and P. Ghosez, Phys. Rev. B **98**, 081108(R) (2018).

[29] O. E. Peil, A. Hampel, C. Ederer, and A. Georges, Phys. Rev. B **99**, 245127 (2019).

[30] J. H. Lee, K. T. Delaney, E. Bousquet, N. A. Spaldin, and K. M. Rabe, Phys. Rev. B **88**, 174426 (2013).

[31] S. Catalano, M. Gibert, V. Bisogni, F. He, R. Sutarto, M. Viret, P. Zubko, R. Scherwitzl, G. A. Sawatzky, T. Schmitt *et al.*, APL Mater. **3**, 062506 (2015).

[32] P. V. Balachandran and J. M. Rondinelli, Phys. Rev. B **88**, 054101 (2013).

[33] J. Axe and M. Crawford, J. Low Temp. Phys. **95**, 271 (1994).

[34] W. E. Pickett, R. E. Cohen, and H. Krakauer, Phys. Rev. Lett. **67**, 228 (1991).

[35] N. L. Saini, A. Lanzara, H. Oyanagi, H. Yamaguchi, K. Oka, T. Ito, and A. Bianconi, Phys. Rev. B **55**, 12759 (1997).

[36] B. Büchner, M. Breuer, A. Freimuth, and A. P. Kampf, Phys. Rev. Lett. **73**, 1841 (1994).

[37] H. Akamatsu, Y. Kumagai, F. Oba, K. Fujita, K. Tanaka, and I. Tanaka, Adv. Funct. Mater. **23**, 1864 (2013).

[38] P. Barone, D. Di Sante, and S. Picozzi, Phys. Rev. B **89**, 144104 (2014).

[39] C. Etz, I. V. Maznichenko, D. Böttcher, J. Henk, A. N. Yaresko, W. Hergert, I. I. Mazin, I. Mertig, and A. Ernst, Phys. Rev. B **86**, 064441 (2012).

[40] R. Hornreich, J. Magn. Magn. Mater. **7**, 280 (1978).

[41] D. Treves, M. Eibschutz, and P. Coppens, Phys. Lett. **18**, 216 (1965).

[42] M. L. Medarde, J. Phys.: Condens. Matter **9**, 1679 (1997).

[43] M. J. Pitcher, P. Mandal, M. S. Dyer, J. Alaria, P. Borisov, H. Niu, J. B. Claridge, and M. J. Rosseinsky, Science **347**, 420 (2015).

[44] S. Das, R. Dokala, B. Weise, R. Medwal, R. Rawat, P. Mishra, and S. Thota, J. Phys.: Condens. Matter **34**, 345803 (2022).

[45] L. Bellaiche, Z. Gui, and I. A. Kornev, J. Phys.: Condens. Matter **24**, 312201 (2012).

[46] J. Blasco, J. L. García-Muñoz, J. García, G. Subías, J. Stankiewicz, J. A. Rodríguez-Velamazán, and C. Ritter, Phys. Rev. B **96**, 024409 (2017).

[47] S. Ishihara, T. Hatakeyama, and S. Maekawa, Phys. Rev. B **65**, 064442 (2002).

[48] L.-J. Yang, Y.-K. Weng, H.-M. Zhang, and S. Dong, J. Phys.: Condens. Matter **26**, 476001 (2014).

[49] D. Li, K. Lee, B. Y. Wang, M. Osada, S. Crossley, H. R. Lee, Y. Cui, Y. Hikita, and H. Y. Hwang, Nature (London) **572**, 624 (2019).

[50] M. Osada, B. Y. Wang, B. H. Goodge, K. Lee, H. Yoon, K. Sakuma, D. Li, M. Miura, L. F. Kourkoutis, and H. Y. Hwang, Nano Lett. **20**, 5735 (2020).

[51] M. Hepting, D. Li, C. Jia, H. Lu, E. Paris, Y. Tseng, X. Feng, M. Osada, E. Been, Y. Hikita *et al.*, Nat. Mater. **19**, 381 (2020).

[52] H. Lu, M. Rossi, A. Nag, M. Osada, D. F. Li, K. Lee, B. Y. Wang, M. Garcia-Fernandez, S. Agrestini, Z. X. Shen, E. M. Been, B. Moritz, T. P. Devereaux, J. Zaanen, H. Y. Hwang, K.-J. Zhou, and W. S. Lee, Science **373**, 213 (2021).

[53] B. Y. Wang, D. Li, B. H. Goodge, K. Lee, M. Osada, S. P. Harvey, L. F. Kourkoutis, M. R. Beasley, and H. Y. Hwang, Nat. Phys. **17**, 473 (2021).

[54] Y. Xiang, Q. Li, Y. Li, H. Yang, Y. Nie, and H.-H. Wen, Chin. Phys. Lett. **38**, 047401 (2021).

[55] D. Li, B. Y. Wang, K. Lee, S. P. Harvey, M. Osada, B. H. Goodge, L. F. Kourkoutis, and H. Y. Hwang, Phys. Rev. Lett. **125**, 027001 (2020).

[56] S. Zeng, C. S. Tang, X. Yin, C. Li, M. Li, Z. Huang, J. Hu, W. Liu, G. J. Omar, H. Jani *et al.*, Phys. Rev. Lett. **125**, 147003 (2020).

[57] F. Lechermann, Phys. Rev. X **10**, 041002 (2020).

[58] F. Lechermann, Phys. Rev. B **101**, 081110(R) (2020).

[59] A. S. Botana and M. R. Norman, Phys. Rev. X **10**, 011024 (2020).

[60] J. Kapeghian and A. S. Botana, Phys. Rev. B **102**, 205130 (2020).

[61] J. Karp, A. S. Botana, M. R. Norman, H. Park, M. Zingl, and A. Millis, Phys. Rev. X **10**, 021061 (2020).

[62] M.-Y. Choi, W. E. Pickett, and K.-W. Lee, Phys. Rev. Res. **2**, 033445 (2020).

[63] E. Been, W.-S. Lee, H. Y. Hwang, Y. Cui, J. Zaanen, T. Devereaux, B. Moritz, and C. Jia, Phys. Rev. X **11**, 011050 (2021).

[64] M.-Y. Choi, K.-W. Lee, and W. E. Pickett, Phys. Rev. B **101**, 020503(R) (2020).

[65] F. Petocchi, V. Christiansson, F. Nilsson, F. Aryasetiawan, and P. Werner, Phys. Rev. X **10**, 041047 (2020).

[66] X. Wan, V. Ivanov, G. Resta, I. Leonov, and S. Y. Savrasov, Phys. Rev. B **103**, 075123 (2021).

[67] I. Leonov, S. Skornyakov, and S. Savrasov, Phys. Rev. B **101**, 241108(R) (2020).

[68] Y. Nomura, M. Hirayama, T. Tadano, Y. Yoshimoto, K. Nakamura, and R. Arita, Phys. Rev. B **100**, 205138 (2019).

[69] C. Xia, J. Wu, Y. Chen, and H. Chen, Phys. Rev. B **105**, 115134 (2022).

[70] F. Bernardini, A. Bosin, and A. Cano, Phys. Rev. Mater. **6**, 044807 (2022).

[71] Á. A. C. Álvarez, S. Petit, L. Iglesias, W. Prellier, M. Bibes, and J. Varignon, Phys. Rev. Res. **4**, 023064 (2022).

[72] A. Subedi, Phys. Rev. Mater. **7**, 024801 (2023).

[73] Y. Zhang, J. Zhang, X. He, J. Wang, and P. Ghosez, PNAS Nexus **2**, pgad108 (2023).

[74] Z. Wang, G.-M. Zhang, Y.-f. Yang, and F.-C. Zhang, Phys. Rev. B **102**, 220501(R) (2020).

[75] B. H. Goodge, D. Li, K. Lee, M. Osada, B. Y. Wang, G. A. Sawatzky, H. Y. Hwang, and L. F. Kourkoutis, Proc. Natl. Acad. Sci. (USA) **118**, e2007683118 (2021).

[76] C. C. Tam, J. Choi, X. Ding, S. Agrestini, A. Nag, M. Wu, B. Huang, H. Luo, P. Gao, M. García-Fernández *et al.*, Nat. Mater. **21**, 1116 (2022).

[77] O. I. Malyi, J. Varignon, and A. Zunger, Phys. Rev. B **105**, 014106 (2022).

[78] J. Fowlie, M. Hadjimichael, M. M. Martins, D. Li, M. Osada, B. Y. Wang, K. Lee, Y. Lee, Z. Salman, T. Prokscha *et al.*, Nat. Phys. **18**, 1043 (2022).

[79] M. Hayward and M. Rosseinsky, Solid State Sci. **5**, 839 (2003).

[80] M. D. Radin, J. C. Thomas, and A. Van der Ven, Phys. Rev. Mater. **4**, 043601 (2020).

[81] I. Levin, F. Yang, R. Maier, W. J. Laws, D. S. Keeble, G. Cibin, and D. C. Sinclair, Adv. Funct. Mater. **30**, 2001840 (2020).

[82] P. Upreti, M. Krogstad, C. Haley, M. Anitescu, V. Rao, L. Poudel, O. Chmaissem, S. Rosenkranz, and R. Osborn, Phys. Rev. Lett. **128**, 095701 (2022).

[83] S. Salmani-Rezaie, K. Ahadi, W. M. Strickland, and S. Stemmer, Phys. Rev. Lett. **125**, 087601 (2020).

[84] S. H. Skjærvø, Q. N. Meier, M. Feygenson, N. A. Spaldin, S. J. L. Billinge, E. S. Bozin, and S. M. Selbach, Phys. Rev. X **9**, 031001 (2019).

[85] Q. Hui, M. G. Tucker, M. T. Dove, S. A. Wells, and D. A. Keen, J. Phys.: Condens. Matter **17**, S111 (2005).

[86] H. Liu, X. Shi, Y. Yao, H. Luo, Q. Li, H. Huang, H. Qi, Y. Zhang, Y. Ren, S. D. Kelly *et al.*, Nat. Commun. **14**, 1007 (2023).

[87] B. Keimer, S. A. Kivelson, M. R. Norman, S. Uchida, and J. Zaanen, Nature (London) **518**, 179 (2015).

[88] J. Zhang, A. Botana, J. Freeland, D. Phelan, H. Zheng, V. Pardo, M. Norman, and J. Mitchell, Nat. Phys. **13**, 864 (2017).

[89] H. Sakakibara, H. Usui, K. Kuroki, R. Arita, and H. Aoki, Phys. Rev. B **85**, 064501 (2012).

[90] G. Kresse and J. Hafner, Phys. Rev. B **47**, 558 (1993).

[91] P. E. Blöchl, Phys. Rev. B **50**, 17953 (1994).

[92] J. P. Perdew, A. Ruzsinszky, G. I. Csonka, O. A. Vydrov, G. E. Scuseria, L. A. Constantin, X. Zhou, and K. Burke, Phys. Rev. Lett. **100**, 136406 (2008).

[93] S. L. Dudarev, G. A. Botton, S. Y. Savrasov, C. J. Humphreys, and A. P. Sutton, Phys. Rev. B **57**, 1505 (1998).

[94] H. J. Monkhorst and J. D. Pack, Phys. Rev. B **13**, 5188 (1976).

[95] X. He, N. Helbig, M. J. Verstraete, and E. Bousquet, Comput. Phys. Commun. **264**, 107938 (2021).

[96] N. Marzari, A. A. Mostofi, J. R. Yates, I. Souza, and D. Vanderbilt, Rev. Mod. Phys. **84**, 1419 (2012).

[97] A. A. Mostofi, J. R. Yates, G. Pizzi, Y.-S. Lee, I. Souza, D. Vanderbilt, and N. Marzari, Comput. Phys. Commun. **185**, 2309 (2014).

[98] H. T. Stokes, D. M. Hatch, B. J. Campbell, and D. E. Tanner, J. Appl. Crystallogr. **39**, 607 (2006).

[99] H. T. Stokes, D. M. Hatch, and B. J. Campbell, ISODISTORT, ISOTROPY Software Suite, iso.byu.edu

[100] I. D. Brown, Chem. Soc. Rev. **7**, 359 (1978).

[101] I. Brown and D. Altermatt, Sect. B: Struct. Sci. **41**, 244 (1985).

[102] N. Brese and M. O'keeffe, Sect. B: Struct. Sci. **47**, 192 (1991).

[103] See Supplemental Material at http://link.aps.org/supplemental/10.1103/PhysRevB.108.165117 for additional figures.

[104] T. Rojac, A. Bencan, G. Drazic, N. Sakamoto, H. Ursic, B. Jancar, G. Tavcar, M. Makarovic, J. Walker, B. Malic *et al.*, Nat. Mater. **16**, 322 (2017).

[105] K. Du, M. Zhang, C. Dai, Z. Zhou, Y. Xie, Z. Ren, H. Tian, L. Chen, G. Van Tendeloo, and Z. Zhang, Nat. Commun. **10**, 1 (2019).

[106] A. M. Glazer, Acta Crystallogr., Sect. B: Struct. Crystallogr. Cryst. Chem. **28**, 3384 (1972).

[107] P. Chen, M. N. Grisolia, H. J. Zhao, O. E. González-Vázquez, L. Bellaiche, M. Bibes, B.-G. Liu, and J. Íñiguez, Phys. Rev. B **97**, 024113 (2018).

[108] W. Zhong and D. Vanderbilt, Phys. Rev. Lett. **74**, 2587 (1995).

[109] N. Sai and D. Vanderbilt, Phys. Rev. B **62**, 13942 (2000).

[110] U. Aschauer and N. A. Spaldin, J. Phys.: Condens. Matter **26**, 122203 (2014).

[111] A. Cammarata and J. M. Rondinelli, J. Chem. Phys. **141**, 114704 (2014).

[112] S. J. May, J.-W. Kim, J. M. Rondinelli, E. Karapetrova, N. A. Spaldin, A. Bhattacharya, and P. J. Ryan, Phys. Rev. B **82**, 014110 (2010).

[113] A. Vailionis, H. Boschker, W. Siemons, E. P. Houwman, D. H. A. Blank, G. Rijnders, and G. Koster, Phys. Rev. B **83**, 064101 (2011).

[114] L. Pauling, J. Am. Chem. Soc. **51**, 1010 (1929).

[115] P. M. Woodward, Acta Crystallogr. Sect. B **53**, 32 (1997).

[116] J. Klarbring and S. I. Simak, Phys. Rev. B **97**, 024108 (2018).

[117] J. C. Wojdeł, P. Hermet, M. P. Ljungberg, P. Ghosez, and J. Iniguez, J. Phys.: Condens. Matter **25**, 305401 (2013).

[118] S. Das, Z. Hong, V. Stoica, M. Gonçalves, Y.-T. Shao, E. Parsonnet, E. J. Marksz, S. Saremi, M. McCarter, A. Reynoso *et al.*, Nat. Mater. **20**, 194 (2021).

[119] F. Gómez-Ortiz, P. García-Fernández, J. M. López, and J. Junquera, Phys. Rev. B **105**, L220103 (2022).

[120] P. Ghosez and J. Junquera, Annu. Rev. Condens. Matter Phys. **13**, 325 (2022).

[121] W. Zhong, D. Vanderbilt, and K. M. Rabe, Phys. Rev. B **52**, 6301 (1995).

[122] W. Zhong, D. Vanderbilt, and K. M. Rabe, Phys. Rev. Lett. **73**, 1861 (1994).

[123] Y. Zhang, X. He, J. Zhang, J. Wang, and P. Ghosez, Adv. Funct. Mater. **33**, 2304187 (2023).